

An Evaluation of Antarctic Sea-Ice Thickness from the Global Ice-Ocean Modeling and Assimilation System based on In situ and Satellite Observations

Sutao Liao¹, Hao Luo^{1*}, Jinfei Wang¹, Qian Shi¹, Jinlun Zhang², Qinghua Yang¹

¹School of Atmospheric Sciences, Sun Yat-sen University, and Southern Marine Science and Engineering Guangdong Laboratory (Zhuhai), Zhuhai, 519082, China

²Polar Science Center, Applied Physics Lab, University of Washington, Seattle, WA 98105

Correspondence to: Hao Luo (luohao25@mail.sysu.edu.cn)

Abstract. Antarctic sea ice is an important component of the Earth system. However, its role in the Earth system is still unclear due to limited Antarctic sea-ice thickness (SIT) data. A reliable sea-ice reanalysis can be useful to study Antarctic SIT and its role in the Earth system. Among various Antarctic sea-ice reanalyses products, the Global Ice-Ocean Modeling and Assimilation System (GIOMAS) output is widely used in the researches of Antarctic sea ice. As more Antarctic SIT observations with quality control are released, a further evaluation of Antarctic SIT from GIOMAS is conducted in this study based on in situ and satellite observations. Generally, though only sea-ice concentration is assimilated, GIOMAS can basically reproduce the observed variability of sea-ice volume and its changes in the trend before and after 2013, indicating that GIOMAS is a good option to study the long-term variation of Antarctic sea ice. However, due to deficiencies in the model and asymmetric changes in SIT caused by assimilation, GIOMAS underestimates Antarctic SIT especially in deformed ice regions, which has an impact on not only the mean state of SIT but also its variability. Thus, besides the further development of the model, assimilating additional sea-ice observations (e.g., SIT and sea-ice drift) with advanced assimilation methods may be conducive to a more accurate estimation of Antarctic SIT.

1 Introduction

Antarctic sea ice plays an important role in the Earth system. Firstly, Antarctic sea ice can influence the Earth climate system. For instance, changes in Antarctic sea ice could affect the freshwater flux of the

26 Southern Ocean that directly influences the stratification of the ocean (Goosse and Zunz, 2014; Haumann
27 et al., 2016). Besides, Antarctic sea ice acts as a protective buffer for Antarctic ice shelves, with the
28 thinning or absence of sea ice increasing the possibility of ice shelf disintegration (Robel, 2017; Massom
29 et al., 2018). Secondly, Antarctic sea ice impacts on the biosphere of the Earth system. Studies have
30 shown that the variation of Antarctic sea-ice thickness (SIT) will affect the maximum biomass of algae
31 in different ice layers, influencing the food web of the Southern Ocean (Massom and Stammerjohn, 2010;
32 Schultz, 2013). Thirdly, Antarctic sea ice impacts on human activities such as shipping and fishery
33 management (Dahood et al., 2019; Mishra et al., 2021). Hence, studies on Antarctic sea ice are of great
34 scientific and socio-economic importance.

35 Although changes in Antarctic sea-ice extent (SIE) have been investigated extensively (Turner et al.,
36 2015; Parkinson, 2019), they may not be a robust proxy of large-scale changes in sea-ice volume (SIV)
37 as the variation of SIV can be considerably different from that of SIE in some regions of the Antarctic
38 (e.g., Kurtz and Markus, 2012). To truly understand changes in sea ice of the Southern Ocean, SIT is
39 needed to estimate the SIV, since it is through volume changes that sea ice has its greatest impact on the
40 water column (Maksym et al., 2012; Hobbs et al., 2016). Many studies related to Antarctic sea ice are
41 limited by the lack of reliable SIT data. For example, the freshwater flux of the Southern Ocean, which
42 affects the stratification of the ocean, cannot be accurately estimated as part of the freshwater flux comes
43 from sea-ice melting and growth (Haumann et al., 2016). In addition, the skill of sea-ice prediction cannot
44 meet the need of human activities in the Antarctic (Mishra et al., 2021). Studies have shown that the skill
45 of Antarctic sea-ice prediction could be improved with better SIT initialization (Bushuk et al., 2021). So
46 far, the commonly used types of the Antarctic SIT data are observations, model data, and reanalyses
47 products and each type of data has its own limitations.

48 Antarctic SIT observations can be divided into in situ and satellite observations. In situ observations can
49 provide the local state of Antarctic SIT. However, the sparse distribution of in situ SIT observations
50 poses considerable challenges to understanding the large-scale characteristics of SIT (Worby et al.,
51 2008a). It is well known that satellite observations have wider spatiotemporal coverage than in situ
52 observations. However, previous studies indicate that there is large uncertainty in SIT data retrieval from
53 satellite altimeters owing to the relatively small total freeboard (i.e., the thickness of sea ice and snow
54 above the sea surface) of Antarctic sea ice compared to that in the Arctic (Maksym and Markus, 2008)
55 and the lack of knowledge about coincident snow cover thickness as well as sea ice and snow density

56 (Alexandrov et al., 2010). In addition, results of numerical simulations are used to investigate the long-
57 term variation of Antarctic SIT (Zhang, 2007; Holland et al., 2014), but discrepancies are identified not
58 only between models and observations but also among models (Shu et al., 2015; Tsujino et al., 2020),
59 indicating the considerable uncertainty in model estimates.

60 It is noted that reanalyses have unique advantages over observed and simulated SIT. Theoretically,
61 reanalyses can provide more accurate or comprehensive state estimations than can otherwise be obtained
62 through either observations or models alone (Buehner et al., 2017). Reanalyses merge the information
63 from both observations and models through data assimilation. Compared with observations, reanalyses
64 data can provide coordinated and gridded data with homogenous sampling in time and space over a long
65 period (Parker, 2016). Besides, compared with model-only data, reanalyses data can produce the state
66 estimations closer to observations because of data assimilation (Lindsay and Zhang, 2006; Rollenhagen
67 et al., 2009). Hence, SIT reanalyses have been widely adopted in studies on the Antarctic sea ice
68 (Abernathey et al., 2016; Kumar et al., 2017). Nevertheless, there are still large uncertainties of present
69 sea-ice reanalyses in the Southern Ocean (Uotila et al., 2019; Shi et al., 2021), suggesting the necessity
70 and importance of evaluation.

71 Among a number of Antarctic sea-ice reanalyses, the Global Ice-Ocean Modeling and Assimilation
72 System (GIOMAS) is one of the most widely used in studies of Antarctic sea ice. For instance, GIOMAS
73 has been regarded as the reference in the assessments of simulations (Shu et al., 2015; Uotila et al., 2017;
74 DuVivier et al., 2020) and predictions (Ordoñez et al., 2018; Morioka et al., 2021). However, GIOMAS
75 has been less widely evaluated, in part because there are far fewer observations of Antarctic SIT against
76 which evaluation is possible (DuVivier et al., 2020).

77 Due to advances in observing technology as well as algorithms in recent years, the quality of Antarctic
78 SIT observations is improved. For example, compared to the European Remote-Sensing Satellites (i.e.,
79 ERS-1 and ERS-2), the Synthetic-Aperture Interferometric Radar Altimeter (SIRAL) on board CryoSat-
80 2 (CS2) is equipped with two radar antennas, which can significantly improve the accuracy of sea-ice
81 freeboard (i.e., thickness of sea ice above the sea surface). CS2 also has a much wider spatial coverage
82 with an enhanced along-track resolution because of the design of the satellite orbit and multiple operation
83 modes (Parrinello et al., 2018). In addition, Paul et al. (2018) developed an adaptive retracker threshold
84 for CS2 to produce consistent sea-ice freeboard data. Besides, more Antarctic SIT observations have
85 been available with the accumulation of observations. For instance, more in situ observations are

86 obtained from dedicated research stations, icebreakers and autonomous underwater vehicles due to
87 increasing research activities in the Antarctic. These progresses provide an opportunity to further
88 evaluate the Antarctic SIT of GIOMAS. Notably, since in situ observations provide relatively accurate
89 estimations in specific points while satellite data provides relatively long and continuous observations
90 with wide spatial coverage, various observations are adopted in the evaluation to make it more
91 comprehensive.

92 The paper is organized as follows. In Sect. 2, Antarctic SIT from GIOMAS and observations are
93 introduced. In Sect. 3, the Antarctic SIT of GIOMAS is evaluated with observations from different
94 aspects, including the climatology, the linear trend, the intensity of variability, as well as the frequency
95 distribution. The final section provides the conclusions and discussion.

96 **2 Data and methods**

97 **2.1 SIT from GIOMAS**

98 GIOMAS consists of a global Parallel Ocean and sea Ice Model (POIM) with data assimilation
99 capabilities, which is developed at the University of Washington (Zhang and Rothrock, 2003). The ocean
100 component of POIM is the Parallel Ocean Program, and the sea-ice component of POIM is the 8-category
101 thickness and enthalpy distribution sea-ice model. The National Centres for Environmental Prediction-
102 National Centre for Atmospheric Research (NCEP-NCAR) daily reanalysis (Kalnay et al., 1996)
103 provides the atmospheric forcing for POIM. Furthermore, in GIOMAS, the modelled sea-ice
104 concentration (SIC) is nudged towards observed SIC derived from Special Sensor Microwave Imager
105 launched by the Defense Meteorological Satellite Program (Weaver et al., 1987), and other modelled
106 variables including SIT are adjusted subsequently. The detailed adjustment process of SIT is as follows:
107 when SIC is nudged in the system, it will modify the SIT distribution to accommodate the change in SIC,
108 which remove sea ice from the distribution without considering its SIT if modelled SIC is too large, while
109 add sea ice to the 0.1-m ice thickness bin if modelled SIC is too small (Lindsay and Zhang, 2006).
110 Compared with modelled SIT without assimilation, this process can reduce the root-mean-square
111 difference and improve the correlation between modelled SIT and observed SIT and it will also cause
112 the thinning of the mean SIT. More technical details for POIM and assimilation procedures can be found
113 in Zhang and Rothrock (2003) and Lindsay and Zhang (2006), respectively. GIOMAS data is available

114 from 1979 to the present with a global coverage and data involved in the assessment spans from January
115 1979 to December 2018 (Fig. 1a). The average horizontal spatial resolution is 0.8 degrees of longitude ×
116 0.8 degrees of latitude (around 60 km × 60 km), and the temporal resolution is one month for all variables.
117 Additionally, GIOMAS also provides daily outputs for some variables, including SIT, SIC and snow
118 depth, and the daily SIT of GIOMAS is assessed in this study. SIT data of GIOMAS is the equivalent
119 SIT, which represents SIV per unit area.

120 **2.2 SIT from satellite altimeters and in situ observations**

121 Satellite-altimeter observations involved in this study are from radar altimeters on-board Envisat (ES)
122 and CS2, which are generated by the Sea Ice Climate Change Initiative (SICCI) project under the
123 European Space Agency Climate Change Initiative (ESA CCI) program. ES was equipped with the Radar
124 Altimeter 2, measuring sea-ice freeboard mainly based on Ku-band frequency (Hendricks et al., 2018b).
125 The Antarctic SIT data derived from ES freeboard spans from December 2002 to November 2011 (Fig.
126 1a) with a coverage of entire Antarctic (Fig. 1b). The spatial resolution is 50 km × 50 km and the temporal
127 resolution is one month. CS2 was equipped with the SIRAL, measuring the sea-ice freeboard mainly
128 based on Ku-band frequency like ES (Hendricks et al., 2018a). CS2 Antarctic SIT dataset spans from
129 November 2010 to April 2017 (Fig. 1a) and the spatial coverage and the spatiotemporal resolution are
130 the same as the ES SIT dataset.

131 In situ SIT observations involved in this study are from upward-looking sonar (ULS), ship-based and
132 air-based measurements. ULS is a kind of mooring measurement at fixed locations, measuring sea-ice
133 draft (thickness of sea ice below the water surface) with a time interval shorter than 15 minutes (Behrendt
134 et al., 2013). Ice draft needs to be converted into total SIT empirically, according to Harms et al. (2001).
135 Thirteen ULSs used in this study were deployed in the Weddell Sea (Fig. 1b) by Alfred Wegener Institute
136 (AWI) and spanned from 1990 to 2010 intermittently (Fig. 1a).

137 The ship-based observations are made up of the Antarctic Sea Ice Processes & Climate program
138 (ASPeCt), ANT-XXIX/6 (Schwegmann, 2013) and ANT-XXIX/7 (Ricker, 2016). The ASPeCt dataset
139 not only includes ASPeCt observations collected from 1981 to 2005 (Worby et al., 2008a), but also
140 includes the ASPeCt bridge-based sea-ice observations collected from 2007 to 2012. The ship tracks
141 cover all sectors of the Southern Ocean (Fig. 1b) and the average spacing of data points is six nautical
142 miles. The air-based SIT observations include data collected by the air-based electromagnetic system

143 (i.e., like an electromagnetic bird carried by helicopter) with a high frequency of 0.5 Hz and an average
144 spacing of 3-4 m (Lemke, 2009, 2014), which is mainly located in the northwest Weddell Sea (Fig. 1b).

145 **2.3 Data processing and methods**

146 According to Parkinson and Cavalieri (2012), the austral summer, autumn, winter and spring in this
147 research refer to January-March, April-June, July-September and October-December, respectively. As
148 shown in Fig. 1b, the Southern Ocean is divided into the Weddell Sea (60° W-20° E), the Indian Ocean
149 (20° E-90°E), the western Pacific Ocean (90°E-160°E), the Ross Sea (160°E-130°W) and the
150 Amundsen/Bellingshausen Sea (130°W-60°W).

151 Since the mismatch in spatial and temporal resolutions between reanalyses and observations could
152 introduce substantial representation errors in the comparisons, the data is processed as Janjić et al. (2018)
153 suggested to eliminate such mismatch between GIOMAS and observations. In general, GIOMAS data is
154 converted to the locations of the observations when compared with satellite and ULS observations while
155 the ship-based and air-based observations are converted to gridded data based on the GIOMAS grid since
156 converting GIOMAS data to the locations of ship-based and air-based observations would introduce
157 considerable errors. For details, when compared with satellite observations, daily GIOMAS data is
158 interpolated to the grid of satellite observations using the linear approach and converted to monthly
159 averages. For the comparisons between GIOMAS and ULS observations, 15-minutely ULS data is
160 converted to daily averages for comparison with daily GIOMAS data and the nearest neighbour approach
161 is used to find the GIOMAS grid cells closest to the ULS locations. Besides, when compared with ship-
162 based and air-based observations, since the observed data is very dense in space and the temporal
163 resolution is always within one day, it is averaged into daily and gridded data based on the GIOMAS
164 grid to create a proper dataset that is compatible with daily GIOMAS SIT data.

165 The climatological annual cycle is defined as the multi-year averages in each month. For observations,
166 the climatological annual cycles are calculated from all years available in each observation dataset. For
167 GIOMAS, when compared with satellite observations, GIOMAS data that coincides with the time spans
168 of satellite observations are selected (2002-2011 for ES and 2010-2017 for CS2) to calculate the
169 climatology. When compared with ULS observations, all years available in GIOMAS (1979-2018) are
170 used for the computation of climatology. Anomalies are defined as departures from the climatological
171 annual cycle, and the intensity of variability is defined as the standard deviation of anomalies. During

172 the overlapping time of ES and CS2 (November 2010 to November 2011), though the difference in SIV
173 anomalies between ES and CS2 (i.e., the root-mean-square error is 473.1 km^3) is not small compared
174 with the mean standard deviation of SIV anomalies (i.e., their standard deviations in ES and CS2 are
175 960.7 km^3 and 956.6 km^3 , respectively), the selection of data in the coincident segment has little effect
176 on the trend. Thus, the SIV anomalies of CS2 during the overlapping time are chosen and ES from
177 December 2002 to October 2010 and CS2 from November 2010 to April 2017 are combined to obtain a
178 relatively long and continuous SIV time series for the linear trend computation. In addition, since the
179 trajectories of air-based SIT observations are mainly distributed in the northwest Weddell Sea which is
180 dominated by deformed sea ice (Fig. 1b), the comparison between GIOMAS and air-based observations
181 is only conducted in the Weddell Sea.

182 **3 Results**

183 **3.1 Comparison in the climatology of SIV and SIT**

184 Figure 2 shows the climatological annual cycle of Antarctic SIV. Although obvious uncertainties of SIV
185 can be found in both ES and CS2, the annual cycle of ES is similar to that of CS2. Both ES and CS2
186 show that the melt rate of sea ice is near twice the growth rate. Besides, there are also some differences
187 in the SIV climatology between ES and CS2. The SIV of CS2 is greater than that of ES in the winter and
188 spring, and larger uncertainties of SIV can be found in ES. The SIV difference between ES and CS2 may
189 be owing to the mismatch in the sea-ice freeboard between ES and CS2. As Paul et al. (2018) indicated,
190 due to the unresolved physical processes such as complex snow metamorphism or sea-ice surface
191 roughness influenced by the flooding in the snow/ice interface, the sea-ice freeboard of ES cannot be
192 well matched with the ones of CS2 in the Antarctic though the retracker algorithms are the same.
193 GIOMAS can reproduce the asymmetry in the annual cycle of Antarctic SIV observed by ES and CS2
194 while underestimating SIV by about 38% on average compared to ES and CS2. Meanwhile, the
195 underestimation is seasonally dependent, with weaker underestimation in summer and stronger one in
196 winter.

197 Figure 3 shows the spatial distribution of SIT bias in summer as well as winter to investigate details of
198 SIV underestimation in these two seasons. In both seasons, significant negative SIT bias of GIOMAS
199 can be found in the deformed ice zone, such as the northwestern Weddell Sea and coasts of the

200 Amundsen/Bellingshausen Sea as well as the coast of East Antarctic. Meanwhile, the extent of negative
201 bias is wider in the winter (Figs. 3b and d) rather than in the summer (Figs. 3a and c), which results in
202 seasonal differences of the SIV underestimation (Fig. 2). In addition, there are weakly positive SIT biases
203 in the southwestern Weddell Sea during winter (Figs. 3b and d), which may be due to model bias in
204 simulating sea-ice transport in the western Weddell Sea (Shi et al., 2021). Considering sea-ice
205 deformation is also related to sea-ice motion tightly, a better simulation of sea-ice motion is required to
206 achieve a more accurate reconstruction of Antarctic SIT. In addition, the relatively large positive bias in
207 winter Ross Sea SIT can only be found in the comparison between GIOMAS and CS2, which may be
208 caused by a smaller freeboard of CS2 than ES in the winter Ross Sea as shown in Paul et al. (2018).
209 Notably, some of the radar altimeter signals would originate from the snow/air interface or from
210 somewhere inside the snow and result in an overestimation of ice freeboard (Willatt et al., 2010; Wang
211 et al., 2020). These uncertainties, combined with often thick snow and complex snow metamorphism in
212 the Antarctic, can contribute to the overestimation of the Antarctic SIT from ES and CS2. Thus, the
213 underestimation of SIT from GIOMAS can be partially attributed to the uncertainties of SIT retrieved
214 from ES and CS2. However, the underestimation in the deformed ice regions can be attributed to the
215 deficiency of GIOMAS since the differences of SIT between GIOMAS and satellite observations in those
216 regions are always larger than the uncertainties of satellite observations.

217 Due to large uncertainties in the above satellite observations, the SIT of GIOMAS is further assessed by
218 ULS measurement in the Weddell Sea. Considering the significant variation of sea ice over horizontal
219 distances as small as a few meters, the standard deviation of ULS is displayed in Fig. 4a. It is obvious
220 that the variability of ULS near the shore (i.e., 206, 207, 212, 217, 232 and 233) is stronger than that of
221 ULS far from the shore (i.e., 208, 209, 210, 227, 229, 230 and 231), indicating larger sea-ice deformation
222 near the shore. As Fig. 4b shows, GIOMAS significantly underestimates the nearshore SIT all year round
223 while slightly overestimates SIT far from the shore in the winter, implying the deficiency of GIOMAS
224 in the simulation of sea-ice deformation, which leads to underestimation of SIT in the Weddell Sea from
225 a perspective of the regional average. The above deficiency of GIOMAS might be attributed to the
226 insufficient resolutions of the model and assimilated SIC observations, which cannot resolve the coastal
227 lines well and hinder GIOMAS from reproducing the ice deformation near shore. Therefore, GIOMAS
228 does underestimate the climatology of Antarctic SIT, mainly in the deformed sea-ice zone, compared
229 with satellite and in situ observations. In addition to the model drawbacks of GIOMAS, this

230 underestimation might also be introduced by the assimilation procedure of GIOMAS. Although only
231 satellite SIC is nudged in GIOMAS, SIT would be adjusted asymmetrically as described in Sect 2.1. This
232 asymmetric addition and removal of ice leads to a thinning of the mean ice thickness (Lindsay and Zhang,
233 2006). Notably, though the uncertainty of satellite observations is large, the differences between
234 GIOMAS and satellite SIT cannot be ignored since the uncertainty of satellite observations is expected
235 to be large owing to the difficulties with the estimation of snow depth and density in the Antarctic (Ozsoy-
236 Cicek et al., 2011; Bunzel et al., 2018).

237 **3.2 Comparison in the trend of SIV**

238 Antarctic SIE shows different trends before and after 2014 (Parkinson, 2019), and SIV better represents
239 the overall changes of sea ice than SIE. Therefore, it is necessary to examine whether there are similar
240 changes in the trend of Antarctic SIV. As Figure 5 shows, the observed Antarctic SIV anomaly increased
241 gradually from 2003, reached the maximum (2783 km³) in November 2013, and then abruptly declined
242 from September 2013 to April 2017. The evolution of SIV anomaly is comparable to that of SIE anomaly,
243 while the time of the SIV anomaly peak is earlier than that of the SIE anomaly peak nearly by one year.
244 The trends of SIV anomalies in the GIOMAS and the observation are 989 and 2968 km³ per month before
245 2013 while -84762 and -119875 km³ per month after 2013, respectively. Although there are differences
246 in the SIV trend between GIOMAS and satellite observation, GIOMAS can basically reproduce the
247 changes in the observed SIV trend before and after 2013. Besides, the correlation of SIV anomalies
248 between GIOMAS and observations is 0.83, which passes a two-tailed t-test at a 99% significant level.
249 Given the advantages of reanalyses over observations or models individually especially in the polar
250 region (Buehner et al., 2017), GIOMAS data would be a good choice to study the variability and long-
251 term trends of Antarctic sea ice.

252 **3.3 Comparison in the intensity of SIT variability**

253 Figure 6 displays spatial differences in the intensity of SIT anomalies variability between GIOMAS and
254 satellite observations. Compared with ES and CS2, GIOMAS underestimates the intensity of SIT
255 variability in the Southern Ocean, especially in the deformed ice zone (Figs. 6a-b), which resembles the
256 spatial pattern of Fig. 3. The underestimation in the deformed ice regions can also be found in the
257 comparison between GIOMAS and ULS. The intensity of SIT variability is underestimated near the shore,

258 while overestimated away from the shore (Fig. 6c). The spatial distribution of differences in the intensity
259 of variability is roughly consistent with that of SIT differences in Fig. 4b. These phenomena suggest that
260 there appears to be a relationship between the mean SIT and the variability. As Blanchard-Wrigglesworth
261 and Bitz (2014) suggested, models with a thinner mean ice state tend to have SIT anomalies with smaller
262 amplitude. In addition, the comparison in SIT standard deviation ratio and mean bias between GIOMAS
263 and satellite observations shown in the supplementary figure further clarifies the relationship that with a
264 negative SIT bias, GIOMAS always underestimates the variability of SIT. Thus, the bias of SIT has an
265 impact not only on the climatology of SIT but also on the variability of SIT. It should be mentioned that
266 in the regions where the uncertainty of satellite observations is larger than the difference between
267 GIOMAS and satellite observations (i.e., mainly in the regions with undeformed sea ice), the uncertainty
268 would have an impact on the evaluation in the variability of SIT and cannot be ignored.

269 **3.4 Comparison of SIT frequency**

270 In addition to ULS observations, the rest of in situ sea-ice observations are sparse in the Southern Ocean
271 and mainly provided by ship-based and air-based measurements. Figure 7 displays the SIT frequency
272 distribution of GIOMAS and ship-based as well as air-based in situ observations. The peaks of
273 observations are mainly around 0-0.6 m while the frequencies of GIOMAS SIT are mainly distributed in
274 0-1.4 m in the Southern Ocean (Fig. 7a). In different sectors (Figs. 7b-f), the frequency distribution of
275 observed SIT data is similar to that in the whole Southern Ocean while the peaks of GIOMAS SIT
276 frequency vary from 0.2 m to 1.4 m. Compared with observations, for the Southern Ocean, GIOMAS
277 has a higher frequency within 0.6-1.6 m while a lower frequency in the rest bins compared with ship-
278 based observations (Fig. 7a), which seems to imply the overestimation of SIT. Similar results can be
279 found in different sectors (Figs. 7b-f). However, the sample selection bias should be noted in the ship-
280 based observations due to the ship's track avoiding areas of thicker ice, which results in its estimation
281 biased toward thinner ice (Timmermann, 2004; Williams et al., 2015). Besides, GIOMAS has a lower
282 frequency of thick ice in the Weddell Sea than air-based observations. In conclusion, GIOMAS tends to
283 overestimate SIT frequency between 0.6-1.6 m in the Southern Ocean compared with ship-based
284 observations under the premise that ship-based observations always bias low. Additionally, the
285 comparison between GIOMAS and air-based SIT observations further proves the weakness of GIOMAS
286 in the simulation of sea-ice deformation.

287 4 Conclusions and discussion

288 Considering the important role of SIT in studies of Antarctic sea ice and the wide application of GIOMAS,
289 the Antarctic SIT of GIOMAS is assessed with satellite and in situ observations. In general, GIOMAS
290 can basically reproduce the observed variability and linear trends of SIV even though only satellite SIC
291 data is assimilated by nudging. For the climatology, GIOMAS can reproduce the asymmetry in the annual
292 cycle of Antarctic SIV. For the long-term SIV variation, the variation of GIOMAS is in phase with that
293 of observations, and it is also able to capture the changes in linear trends before and after 2013. These
294 suggest that GIOMAS is useful to study the long-term variation of Antarctic sea ice. However, significant
295 negative bias in SIT can be found in the comparison between GIOMAS and observations. Compared
296 with satellite measurements, GIOMAS tends to underestimate SIT, especially in regions with strong ice
297 deformation. This underestimation is of seasonal dependence with greater underestimation in the winter.
298 Although the above underestimation can be partially attributed to the uncertainties of SIT retrieved from
299 satellite, the SIT underestimation cannot be ignored in the northwest Weddell Sea and is further verified
300 by the comparison between GIOMAS and ULS observations. Furthermore, the spatial distribution of the
301 differences in the magnitude of SIT variability resembles that of the differences in SIT climatology
302 between GIOMAS and observations. Given the relationship between the mean state of SIT and variability
303 (Blanchard-Wrigglesworth and Bitz, 2014; also verified by the comparison between satellite
304 observations and GIOMAS in the supplement), this phenomenon indicates that SIT underestimation
305 might have an impact on not only the SIT climatology but also the SIT variability. In addition, GIOMAS
306 overestimates SIT compared with ship-based observations, which can be due to the negative bias in ship-
307 based SIT estimation (Timmermann, 2004; Williams et al., 2015). The deficiency of GIOMAS in
308 simulating deformed sea ice is further verified in comparison with air-based observations.
309 Notably, though GIOMAS could basically reproduce the trends of Antarctic SIV anomalies before and
310 after 2013, the differences in the trends of SIV anomalies between GIOMAS and satellite observations
311 cannot be ignored. A simple comparison between the monthly GIOMAS sea-surface temperature (SST)
312 and Microwave Optimally Interpolated SST observations reveals that the positive bias of GIOMAS in
313 SST before 2014 is roughly corresponding to the underestimation of the positive trend of observed SIV
314 anomalies while the negative SST bias of GIOMAS after 2014 is corresponding to the underestimation
315 of the negative trend of observed SIV anomalies. There seems to be a possible relationship between the

316 difference in SST and the difference in the trends of SIV anomalies between GIOMAS and observations
317 since higher SST would slow down the increase of SIV while lower SST would slow down the decrease
318 of SIV. However, this relationship needs further quantification and further analysis is added to our future
319 work plan.

320 In addition, limitations from Antarctic SIT observations are non-negligible in this study. For one aspect,
321 the scarcity of Antarctic SIT observations is one of the main sources of limitations for the evaluation.
322 The time span of satellite observations is not long enough for the evaluation of GIOMAS SIT data from
323 1979 to the present while the in situ observations are too few to show the estimation of SIT in the entire
324 Southern Ocean. Those make it unable to comprehensively evaluate the entire GIOMAS Antarctic SIT
325 data in this study. For another, this study is also limited by observations of Antarctic SIT due to their
326 unsuitability for the evaluation. For example, though SIT from ICESat (Kern et al., 2016) equipped with
327 the Geoscience Laser Altimeter System is available from 2004 to 2008 and proved to have a lower bias
328 in SIT estimation than radar altimeter measurements (Willatt et al., 2010; Wang et al., 2020), it is not
329 adopted in this study. The reasons are as follows. First, ICESat SIT is not available in winter (July-
330 September), when a greater underestimation of SIT is found in GIOMAS (Fig. 2). Second, the data size
331 of ICESat is relatively smaller than that of ES and CS2 because ICESat provides seasonal mean data and
332 its time range is narrower. Therefore, the additional assessment on SIT of GIOMAS will be conducted
333 when the Antarctic SIT derived from ICESat-2 is available. Furthermore, the uncertainty of satellite
334 observations has an impact on the evaluation and the accuracy of satellite observations needs to be further
335 improved to obtain more accurate satellite-derived SIT estimations with smaller uncertainty. The
336 uncertainty of satellite-derived SIT observations is mainly from the uncertainty introduced by the
337 scattering surface of radar signals and the estimation of Antarctic snow depth and density. With the
338 influences of complex snow stratigraphy and flooding inside the snow related to the formation of snow
339 ice, the assumption that the radar signal reflects from the snow/ice interface is not applicable in most
340 cases (Willatt et al., 2010). Besides, owing to the lack of knowledge of Antarctic snow, the climatology
341 of snow depth from the European Space Agency-SICCI Advanced Microwave Scanning Radiometer for
342 the Earth Observing System (AMSR-E) and the Advanced Microwave Scanning Radiometer 2 (AMSR2)
343 is used in the retrieval of ES and CS2-derived SIT, which would introduce extra uncertainties since the
344 inter-annual variability in snow depth is omitted (Bunzel et al., 2018). Moreover, the AMSR-E/AMSR2
345 snow depth is indicated to considerably underestimate the actual snow depth, which usually occurs in

346 the East Antarctic (Worby et al., 2008b; Ozsoy-Cicek et al., 2011). All those contribute to the large
347 uncertainty of the satellite-derived SIT in the Antarctic and the uncertainty would influence the
348 evaluation of SIT in the regions where the differences between GIOMAS SIT and satellite observations
349 are smaller than the uncertainty. Therefore, a more accurate estimation of Antarctic snow depth and
350 density would be essential to reducing the uncertainty of satellite SIT observations and thus improving
351 the reliability of the evaluation.

352 The above SIT underestimation of GIOMAS can be partially attributed to the model weakness. For
353 example, insufficient resolution of the model restricts GIOMAS to reproduce the ice deformation near
354 shore. Besides, the assimilation is a vital component in the reanalyses since it could constraint the model
355 with observations and make the model obtain better state estimation (Lahoz and Schneider, 2014).
356 However, it can also be a source of errors in the system. In GIOMAS, the asymmetric SIT changes
357 introduced by assimilation cannot be ignored. Thus, besides the further development of the model, there
358 are two suggested ways to improve the estimation of Antarctic SIT from the perspective of data
359 assimilation. Firstly, additional sea-ice observations other than SIC should be assimilated. For example,
360 besides Antarctic SIT derived from Envisat and CryoSat-2 used in this study, the Antarctic SIT retrieved
361 from ICESat-2 is also to be released in the near future, and hence assimilating these SIT observations
362 directly may suppress the bias of SIT (e.g., Yang et al., 2014; Fritzner et al., 2019; Luo et al., 2021). Also,
363 assimilating sea-ice drift observations can improve the simulation of sea-ice motion and deformation,
364 which can improve the estimation of SIT (e.g., Lindsay and Zhang, 2006; Mu et al., 2020). Secondly,
365 advanced data assimilation methods should be adopted to provide a balanced estimation of the model
366 state. For instance, the innovation of SIC can be converted to the increment of SIT in a more balanced
367 way through the flow-dependent covariance of Ensemble Kalman Filter (e.g., Massonnet et al., 2013;
368 Yang et al., 2015). Furthermore, though nudging of SIC is not state of the art, it makes the model of
369 GIOMAS obtain better SIT simulation while the model-only data of GIOMAS is likely to overestimate
370 SIT in the marginal seas. To promote the development of GIOMAS, further quantitative analyses on the
371 impact of nudging SIC on the SIT in the Antarctic are worthy of attention and will be conducted in the
372 future.

373 Besides, in the course of global warming, Antarctic SIE rose gradually and reached a record high in
374 2014/2015 before decreasing dramatically, which is obviously different from the dramatic drop in Arctic
375 SIE during the satellite era (e.g., Turner and Comiso, 2017). Results from a recent study suggest that the

376 trend in Antarctic ice coverage may be due to changes in atmospheric (e.g., Holland and Kwok, 2012)
377 and oceanic (e.g., Meehl et al., 2019) processes. Without better SIT and SIV estimates, it is difficult to
378 characterize how Antarctic sea-ice cover is responding to changing climate, or which climate parameters
379 are most influential (Vaughan et al., 2013). Thus, more Antarctic sea-ice observations and more studies
380 on data assimilation are urgently needed to accurately evaluate the Antarctic SIT, which can help to
381 improve the reconstruction and prediction of Antarctic SIV and to support research related to Antarctic
382 sea ice.

383 **Data availability**

384 The GIOMAS reanalysis data are available at
385 http://psc.apl.washington.edu/zhang/Global_seaice/data.html. The satellite-based Antarctic sea ice
386 thickness observations from Envisat and CryoSat-2 are available at
387 <https://doi.org/10.5285/b1f1ac03077b4aa784c5a413a2210bf5> and
388 <https://doi.org/10.5285/48fc3d1e8ada405c8486ada522dae9e8>, respectively. The Weddell Sea upward-
389 looking sonar sea ice draft data are available at <https://doi.pangaea.de/10.1594/PANGAEA.785565>. The
390 ship-based sea ice thickness observations are available at <http://aspect.antarctica.gov.au/data>,
391 <https://doi.org/10.1594/PANGAEA.819540> and <https://doi.org/10.1594/PANGAEA.831976>. The sea ice
392 thickness observations from airborne electromagnetic system are freely available at
393 <https://doi.pangaea.de/10.1594/PANGAEA.771229> and <https://epic.awi.de/id/eprint/36245/>.

394 **Author contribution**

395 QY and HL developed the concept of the paper. SL and HL performed analysis and drafted the manuscript.
396 JW collected the remote sensing and observation data. QY, JZ, QS and JW gave comments and helped
397 revise the manuscript. All of the coauthors contributed to scientific interpretations.

398 **Competing interests**

399 The authors declare that they have no conflict of interest.

400 **Acknowledgments**

401 This study is supported by the National Natural Science Foundation of China (No. 41941009, 41922044,
402 42006191), and the Guangdong Basic and Applied Basic Research Foundation (No. 2020B1515020025).
403 This is a contribution to the Year of Polar Prediction (YOPP), a flagship activity of the Polar Prediction
404 Project (PPP), initiated by the World Weather Research Programme (WWRP) of the World
405 Meteorological Organisation (WMO). We acknowledge the WMO WWRP for its role in coordinating
406 this international research activity.

407 **References**

- 408 Abernathy, R. P., Cerovecki, I., Holland, P. R., Newsom, E., Mazloff, M., and Talley, L. D.: Water-
409 mass transformation by sea ice in the upper branch of the Southern Ocean overturning, *Nat. Geosci.*, 9,
410 596-601, <https://doi.org/10.1038/ngeo2749>, 2016.
- 411 Alexandrov, V., Sandven, S., Wahlin, J., and Johannessen, O. M.: The relation between sea ice thickness
412 and freeboard in the Arctic, *The Cryosphere*, 4, 373-380, <https://doi.org/10.5194/tc-4-373-2010>, 2010.
- 413 Behrendt, A., Dierking, W., Fahrbach, E., and Witte, H.: Sea ice draft in the Weddell Sea, measured by
414 upward looking sonars, *Earth Syst. Sci. Data*, 5, 209-226, <https://doi.org/10.5194/essd-5-209-2013>, 2013.
- 415 Blanchard-Wrigglesworth, E., and Bitz, C. M.: Characteristics of Arctic Sea-Ice Thickness Variability
416 in GCMs, *J. Climate*, 27, 8244-8258, <https://doi.org/10.1175/jcli-d-14-00345.1>, 2014.
- 417 Buehner, M., Bertino, L., Caya, A., Heimbach, P., and Smith, G.: Sea Ice Data Assimilation, in: *Sea Ice*
418 *Analysis and Forecasting: Towards an Increased Reliance on Automated Prediction Systems*, edited by:
419 Lemieux, J.-F., Toudal Pedersen, L., Buehner, M., and Carrieres, T., Cambridge University Press,
420 Cambridge, 51-108, <https://doi.org/10.1017/9781108277600.005>, 2017.
- 421 Bunzel, F., Notz, D., and Pedersen, L. T.: Retrievals of Arctic Sea-Ice Volume and Its Trend Significantly
422 Affected by Interannual Snow Variability, *Geophysical Research Letters*, 45, 11,751-711,759,
423 <https://doi.org/10.1029/2018GL078867>, 2018.
- 424 Bushuk, M., Winton, M., Haumann, F. A., Delworth, T., Lu, F., Zhang, Y., Jia, L., Zhang, L., Cooke,
425 W., Harrison, M., Hurlin, B., Johnson, N. C., Kapnick, S., McHugh, C., Murakami, H., Rosati, A., Tseng,
426 K.-C., Wittenberg, A. T., Yang, X., and Zeng, F.: Seasonal prediction and predictability of regional
427 Antarctic sea ice, *J. Climate*, 1-68, <https://doi.org/10.1175/jcli-d-20-0965.1>, 2021.
- 428 Dahood, A., Watters, G. M., and de Mutsert, K.: Using sea-ice to calibrate a dynamic trophic model for
429 the Western Antarctic Peninsula, *PloS One*, 14, e0214814, <https://doi.org/10.1371/journal.pone.0214814>,
430 2019.
- 431 DuVivier, A. K., Holland, M. M., Kay, J. E., Tilmes, S., Gettelman, A., and Bailey, D. A.: Arctic and
432 Antarctic Sea Ice Mean State in the Community Earth System Model Version 2 and the Influence of
433 Atmospheric Chemistry, *J. Geophys. Res.-Oceans*, 125, e2019JC015934,
434 <https://doi.org/10.1029/2019JC015934>, 2020.
- 435 Fritzner, S., Graverson, R., Christensen, K. H., Rostosky, P., and Wang, K.: Impact of assimilating sea
436 ice concentration, sea ice thickness and snow depth in a coupled ocean-sea ice modelling system, *The*
437 *Cryosphere*, 13, 491-509, <https://doi.org/10.5194/tc-13-491-2019>, 2019.

438 Goosse, H., and Zunz, V.: Decadal trends in the Antarctic sea ice extent ultimately controlled by ice–
439 ocean feedback, *The Cryosphere*, 8, 453–470, <https://doi.org/10.5194/tc-8-453-2014>, 2014.

440 Harms, S., Fahrbach, E., and Strass, V. H.: Sea ice transports in the Weddell Sea, *J. Geophys. Res.-Oceans*,
441 106, 9057–9073, <https://doi.org/10.1029/1999jc000027>, 2001.

442 Haumann, F. A., Gruber, N., Münnich, M., Frenger, I., and Kern, S.: Sea-ice transport driving Southern
443 Ocean salinity and its recent trends, *Nature*, 537, 89–92, <https://doi.org/10.1038/nature19101>, 2016.

444 Hendricks, S., Paul, S., and Rinne, E.: ESA Sea Ice Climate Change Initiative (Sea_Ice_cci): Southern
445 hemisphere sea ice thickness from the CryoSat-2 satellite on a monthly grid (L3C), v2.0, Centre for
446 Environmental Data Analysis, <https://doi.org/10.5285/48fc3d1e8ada405c8486ada522dae9e8>, 2018a.

447 Hendricks, S., Paul, S., and Rinne, E.: ESA Sea Ice Climate Change Initiative (Sea_Ice_cci): Southern
448 hemisphere sea ice thickness from the Envisat satellite on a monthly grid (L3C), v2.0,
449 <https://doi.org/10.5285/b1f1ac03077b4aa784c5a413a2210bf5>, 2018b.

450 Hobbs, W. R., Massom, R., Stammerjohn, S., Reid, P., Williams, G., and Meier, W.: A review of recent
451 changes in Southern Ocean sea ice, their drivers and forcings, *Global Planet. Change*, 143, 228–250,
452 <https://doi.org/10.1016/j.gloplacha.2016.06.008>, 2016.

453 Holland, P. R., and Kwok, R.: Wind-driven trends in Antarctic sea-ice drift, *Nat. Geosci.*, 5, 872–875,
454 <https://doi.org/10.1038/ngeo1627>, 2012.

455 Holland, P. R., Bruneau, N., Enright, C., Losch, M., Kurtz, N. T., and Kwok, R.: Modeled Trends in
456 Antarctic Sea Ice Thickness, *J. Climate*, 27, 3784–3801, <https://doi.org/10.1175/jcli-d-13-00301.1>, 2014.

457 Kalnay, E., Kanamitsu, M., Kistler, R., Collins, W., Deaven, D., Gandin, L., Iredell, M., Saha, S., White,
458 G., Woollen, J., Zhu, Y., Chelliah, M., Ebisuzaki, W., Higgins, W., Janowiak, J., Mo, K. C., Ropelewski,
459 C., Wang, J., Leetmaa, A., Reynolds, R., Jenne, R., and Joseph, D.: The NCEP/NCAR 40-year reanalysis
460 project, *B. Am. Meteorol. Soc.*, 77, 437–471, [https://doi.org/10.1175/1520-0477\(1996\)077<0437:tnyrp>2.0.co;2](https://doi.org/10.1175/1520-0477(1996)077<0437:tnyrp>2.0.co;2), 1996.

461 Janjić, T., Bormann, N., Bocquet, M., Carton, J. A., Cohn, S. E., Dance, S. L., Losa, S. N., Nichols, N.
462 K., Potthast, R., Waller, J. A., and Weston, P.: On the representation error in data assimilation, *Quarterly*
463 *Journal of the Royal Meteorological Society*, 144, 1257–1278, <https://doi.org/10.1002/qj.3130>, 2018.

464 Kern, S., Ozsoy-Çiçek, B., and Worby, A.: Antarctic Sea-Ice Thickness Retrieval from ICESat: Inter-
465 Comparison of Different Approaches, *Remote Sens.-Basel*, 8, <https://doi.org/10.3390/rs8070538>, 2016.

466 Kumar, A., Dwivedi, S., and Rajak, D. R.: Ocean sea-ice modelling in the Southern Ocean around Indian
467 Antarctic stations, *Journal of Earth System Science*, 126, 70, [https://doi.org/10.1007/s12040-017-0848-](https://doi.org/10.1007/s12040-017-0848-5)
468 [5](https://doi.org/10.1007/s12040-017-0848-5), 2017.

469 Kurtz, N. T. and Markus, T.: Satellite observations of Antarctic sea ice thickness and volume, *Journal of*
470 *Geophysical Research: Oceans*, 117, <https://doi.org/10.1029/2012JC008141>, 2012.

471 Lahoz, W. A. and Schneider, P.: Data assimilation: making sense of Earth Observation, *Frontiers in*
472 *Environmental Science*, 2, 10.3389/fenvs.2014.00016, 2014.

473 Lemke, P.: The Expedition of the Research Vessel Polarstern to the Antarctic in 2006 (ANT-XXIII/7),
474 Alfred-Wegener-Institut für Polar- und Meeresforschung;, Bremerhaven, Germany1866-3192, 1–147,
475 2009.

476 Lemke, P.: The Expedition of the Research Vessel Polarstern to the Antarctic in 2013 (ANT-XXIX/6),
477 Alfred-Wegener-Institut, Helmholtz-Zentrum für Polar- und Meeresforschung;, Bremerhaven,
478 Germany1866-3192, 1–154, 2014.

479 Lindsay, R. W., and Zhang, J.: Assimilation of ice concentration in an ice–ocean model, *J. Atmos. Ocean.*
480 *Tech.*, 23, 742–749, <https://doi.org/10.1175/jtech1871.1>, 2006.

481

482 Luo, H., Yang, Q., Mu, L., Tian-Kunze, X., Nerger, L., Mazloff, M., Kaleschke, L., and Chen, D.:
483 DASSO: a data assimilation system for the Southern Ocean that utilizes both sea-ice concentration and
484 thickness observations, *J. Glaciol.*, 1-6, <https://doi.org/10.1017/jog.2021.57>, 2021.

485 Maksym, T., and Markus, T.: Antarctic sea ice thickness and snow-to-ice conversion from atmospheric
486 reanalysis and passive microwave snow depth, *J. Geophys. Res.*, 113,
487 <https://doi.org/10.1029/2006jc004085>, 2008.

488 Maksym, T., Stammerjohn, S., Ackley, S., and Massom, R.: Antarctic Sea Ice—A Polar Opposite?,
489 *Oceanography*, 25, 140-151, <https://doi.org/10.5670/oceanog.2012.88>, 2012.

490 Massom, R. A., and Stammerjohn, S. E.: Antarctic sea ice change and variability – Physical and
491 ecological implications, *Polar Sci.*, 4, 149-186, <https://doi.org/10.1016/j.polar.2010.05.001>, 2010.

492 Massom, R. A., Scambos, T. A., Bennetts, L. G., Reid, P., Squire, V. A., and Stammerjohn, S. E.:
493 Antarctic ice shelf disintegration triggered by sea ice loss and ocean swell, *Nature*, 558, 383-389,
494 <https://doi.org/10.1038/s41586-018-0212-1>, 2018.

495 Massonnet, F., Mathiot, P., Fichet, T., Goosse, H., Beatty, C. K., Vancoppenolle, M., and Lavergne,
496 T.: A model reconstruction of the Antarctic sea ice thickness and volume changes over 1980-2008 using
497 data assimilation, *Ocean Model.*, 64, 67-75, <https://doi.org/10.1016/j.ocemod.2013.01.003>, 2013.

498 Meehl, G. A., Arblaster, J. M., Chung, C. T. Y., Holland, M. M., DuVivier, A., Thompson, L., Yang, D.,
499 and Bitz, C. M.: Sustained ocean changes contributed to sudden Antarctic sea ice retreat in late 2016,
500 *Nat. Commun.*, 10, 14, <https://doi.org/10.1038/s41467-018-07865-9>, 2019.

501 Mishra, P., Alok, S., Rajak, D. R., Beg, J. M., Bahuguna, I. M., and Talati, I.: Investigating optimum
502 ship route in the Antarctic in presence of sea ice and wind resistances – A case study between Bharati
503 and Maitri, *Polar Sci.*, <https://doi.org/10.1016/j.polar.2021.100696>, 2021.

504 Morioka, Y., Iovino, D., Cipollone, A., Masina, S., and Behera, S. K.: Summertime sea-ice prediction in
505 the Weddell Sea improved by sea-ice thickness initialization, *Sci. Rep.-UK*, 11, 11475,
506 <https://doi.org/10.1038/s41598-021-91042-4>, 2021.

507 Mu, L., Nerger, L., Tang, Q., Loza, S. N., Sidorenko, D., Wang, Q., Semmler, T., Zampieri, L., Losch,
508 M., and Goessling, H. F.: Toward a data assimilation system for seamless sea ice prediction based on the
509 AWI climate model, *J. Adv. Model. Earth. Sy.*, 12, e2019MS001937,
510 <https://doi.org/10.1029/2019ms001937>, 2020.

511 Ordoñez, A. C., Bitz, C. M., and Blanchard-Wrigglesworth, E.: Processes controlling Arctic and
512 Antarctic sea ice predictability in the Community Earth System Model, *J. Climate*, 31, 9771-9786,
513 <https://doi.org/10.1175/jcli-d-18-0348.1>, 2018.

514 Ozsoy-Cicek, B., Kern, S., Ackley, S. F., Xie, H., and Tekeli, A. E.: Intercomparisons of Antarctic sea
515 ice types from visual ship, RADARSAT-1 SAR, Envisat ASAR, QuikSCAT, and AMSR-E satellite
516 observations in the Bellingshausen Sea, *Deep Sea Research Part II: Topical Studies in Oceanography*,
517 58, 1092-1111, <https://doi.org/10.1016/j.dsr2.2010.10.031>, 2011.

518 Parker, W. S.: Reanalyses and observations: What's the difference?, *B. Am. Meteorol. Soc.*, 97, 1565-
519 1572, <https://doi.org/10.1175/bams-d-14-00226.1>, 2016.

520 Parkinson, C. L., and Cavalieri, D. J.: Antarctic sea ice variability and trends, 1979–2010, *The
521 Cryosphere*, 6, 871-880, <https://doi.org/10.5194/tc-6-871-2012>, 2012.

522 Parkinson, C. L.: A 40-y record reveals gradual Antarctic sea ice increases followed by decreases at rates
523 far exceeding the rates seen in the Arctic, *P. Natl. Acad. Sci. USA*, 116, 14414-14423,
524 <https://doi.org/10.1073/pnas.1906556116>, 2019.

525 Parrinello, T., Shepherd, A., Bouffard, J., Badessi, S., Casal, T., Davidson, M., Fornari, M., Maestroni,
526 E., and Scagliola, M.: CryoSat: ESA's ice mission – Eight years in space, *Adv. Space Res.*, 62, 1178-
527 1190, <https://doi.org/10.1016/j.asr.2018.04.014>, 2018.

528 Paul, S., Hendricks, S., Ricker, R., Kern, S., and Rinne, E.: Empirical parametrization of Envisat
529 freeboard retrieval of Arctic and Antarctic sea ice based on CryoSat-2: progress in the ESA Climate
530 Change Initiative, *The Cryosphere*, 12, 2437-2460, <https://doi.org/10.5194/tc-12-2437-2018>, 2018.

531 Ricker, R.: Sea ice conditions during POLARSTERN cruise ANT-XXIX/7, PANGAEA,
532 <https://doi.org/10.1594/PANGAEA.831976>, 2016.

533 Robel, A. A.: Thinning sea ice weakens buttressing force of iceberg mélange and promotes calving, *Nat.*
534 *Commun.*, 8, 14596, <https://doi.org/10.1038/ncomms14596>, 2017.

535 Rollenhagen, K., Timmermann, R., Janjić, T., Schröter, J., and Danilov, S.: Assimilation of sea ice
536 motion in a finite-element sea ice model, *J. Geophys. Res.*, 114, <https://doi.org/10.1029/2008jc005067>,
537 2009.

538 Schultz, C.: Antarctic sea ice thickness affects algae populations, *Eos Trans. AGU*, 94, 40-40,
539 <https://doi.org/10.1002/2013EO030032>, 2013.

540 Schwegmann, S.: Sea ice conditions during POLARSTERN cruise ANT-XXIX/6 (AWECS),
541 PANGAEA, <https://doi.org/10.1594/PANGAEA.819540>, 2013.

542 Shi, Q., Yang, Q., Mu, L., Wang, J., Massonnet, F., and Mazloff, M. R.: Evaluation of sea-ice thickness
543 from four reanalyses in the Antarctic Weddell Sea, *The Cryosphere*, 15, 31-47,
544 <https://doi.org/10.5194/tc-15-31-2021>, 2021.

545 Shu, Q., Song, Z.-Y., and Qiao, F.-L.: Assessment of sea ice simulations in the CMIP5 models, *The*
546 *Cryosphere*, 9, 399-409, <https://doi.org/10.5194/tc-9-399-2015>, 2015.

547 Timmermann, R.: Utilizing the ASPeCt sea ice thickness data set to evaluate a global coupled sea ice–
548 ocean model, *J. Geophys. Res.*, 109, <https://doi.org/10.1029/2003jc002242>, 2004.

549 Tsujino, H., Urakawa, L. S., Griffies, S. M., Danabasoglu, G., Adcroft, A. J., Amaral, A. E., Arsouze, T.,
550 Bentsen, M., Bernardello, R., Böning, C. W., Bozec, A., Chassignet, E. P., Danilov, S., Dussin, R.,
551 Exarchou, E., Fogli, P. G., Fox-Kemper, B., Guo, C., Ilicak, M., Iovino, D., Kim, W. M., Koldunov, N.,
552 Lapin, V., Li, Y., Lin, P., Lindsay, K., Liu, H., Long, M. C., Komuro, Y., Marsland, S. J., Masina, S.,
553 Nummelin, A., Rieck, J. K., Ruprich-Robert, Y., Scheinert, M., Sicardi, V., Sidorenko, D., Suzuki, T.,
554 Tatebe, H., Wang, Q., Yeager, S. G., and Yu, Z.: Evaluation of global ocean–sea-ice model simulations
555 based on the experimental protocols of the Ocean Model Intercomparison Project phase 2 (OMIP-2),
556 *Geosci. Model Dev.*, 13, 3643-3708, <https://doi.org/10.5194/gmd-13-3643-2020>, 2020.

557 Turner, J., Hosking, J. S., Bracegirdle, T. J., Marshall, G. J., and Phillips, T.: Recent changes in Antarctic
558 Sea Ice, *Philos. Trans. A Math. Phys. Eng. Sci.*, 373, <https://doi.org/10.1098/rsta.2014.0163>, 2015.

559 Turner, J., and Comiso, J.: Solve Antarctica's sea-ice puzzle, *Nature*, 547, 275-277,
560 <https://doi.org/10.1038/547275a>, 2017.

561 Uotila, P., Iovino, D., Vancoppenolle, M., Lensu, M., and Rousset, C.: Comparing sea ice, hydrography
562 and circulation between NEMO3.6 LIM3 and LIM2, *Geosci. Model Dev.*, 10, 1009-1031,
563 <https://doi.org/10.5194/gmd-10-1009-2017>, 2017.

564 Uotila, P., Goosse, H., Haines, K., Chevallier, M., Barthélemy, A., Bricaud, C., Carton, J., Fučkar, N.,
565 Garric, G., Iovino, D., Kauker, F., Korhonen, M., Lien, V. S., Marnela, M., Massonnet, F., Mignac, D.,
566 Peterson, K. A., Sadikni, R., Shi, L., Tietsche, S., Toyoda, T., Xie, J., and Zhang, Z.: An assessment of
567 ten ocean reanalyses in the polar regions, *Clim. Dyn.*, 52, 1613-1650, [https://doi.org/10.1007/s00382-](https://doi.org/10.1007/s00382-018-4242-z)
568 018-4242-z, 2019.

569 Vaughan, D. G., Comiso, J. C., Allison, I., Carrasco, J., Kaser, G., Kwok, R., Mote, P., Murray, T., Paul,
570 F., Ren, J.-W., E. Rignot, E., Solomina, O., Steffen, K., and Zhang, T.-J.: Observations: Cryosphere, in:
571 Climate change 2013: The physical science basis. Contribution of working group I to the fifth assessment
572 report of the intergovernmental panel on climate change, edited by: Stocker, T. F., Qin, D.-H., Plattner,
573 G.-K., Tignor, M., Allen, S. K., Boschung, J., Nauels, A., Xia, Y., Bex, V., and Midgley, P. M.,
574 Cambridge University Press, Cambridge, United Kingdom and New York, NY, USA, 317-382,
575 <https://doi.org/10.1017/CBO9781107415324.012>, 2013.

576 Wang, J., Min, C., Ricker, R., Yang, Q., Shi, Q., Han, B., and Hendricks, S.: A comparison between
577 Envisat and ICESat sea ice thickness in the Antarctic, *The Cryosphere Discuss.*, 2020, 1-26,
578 <https://doi.org/10.5194/tc-2020-48>, 2020.

579 Weaver, R., Morris, C., and Barry, R. G.: Passive microwave data for snow and ice research: Planned
580 products from the DMSP SSM/I System, *Eos Trans. AGU*, 68, 769-777,
581 <https://doi.org/10.1029/EO068i039p00769>, 1987.

582 Willatt, R. C., Giles, K. A., Laxon, S. W., Stone-Drake, L., and Worby, A. P.: Field Investigations of
583 Ku-Band Radar Penetration Into Snow Cover on Antarctic Sea Ice, *IEEE T. Geosci. Remote*, 48, 365-
584 372, <https://doi.org/10.1109/TGRS.2009.2028237>, 2010.

585 Williams, G., Maksym, T., Wilkinson, J., Kunz, C., Murphy, C., Kimball, P., and Singh, H.: Thick and
586 deformed Antarctic sea ice mapped with autonomous underwater vehicles, *Nat. Geosci.*, 8, 61-67,
587 <https://doi.org/10.1038/ngeo2299>, 2015.

588 Worby, A. P., Geiger, C. A., Paget, M. J., Van Woert, M. L., Ackley, S. F., and DeLiberty, T. L.:
589 Thickness distribution of Antarctic sea ice, *J. Geophys. Res.-Oceans*, 113,
590 <https://doi.org/10.1029/2007JC004254>, 2008a.

591 Worby, A. P., Markus, T., Steer, A. D., Lytle, V. I., and Massom, R. A.: Evaluation of AMSR-E snow
592 depth product over East Antarctic sea ice using in situ measurements and aerial photography, *Journal of*
593 *Geophysical Research: Oceans*, 113, <https://doi.org/10.1029/2007JC004181>, 2008b.

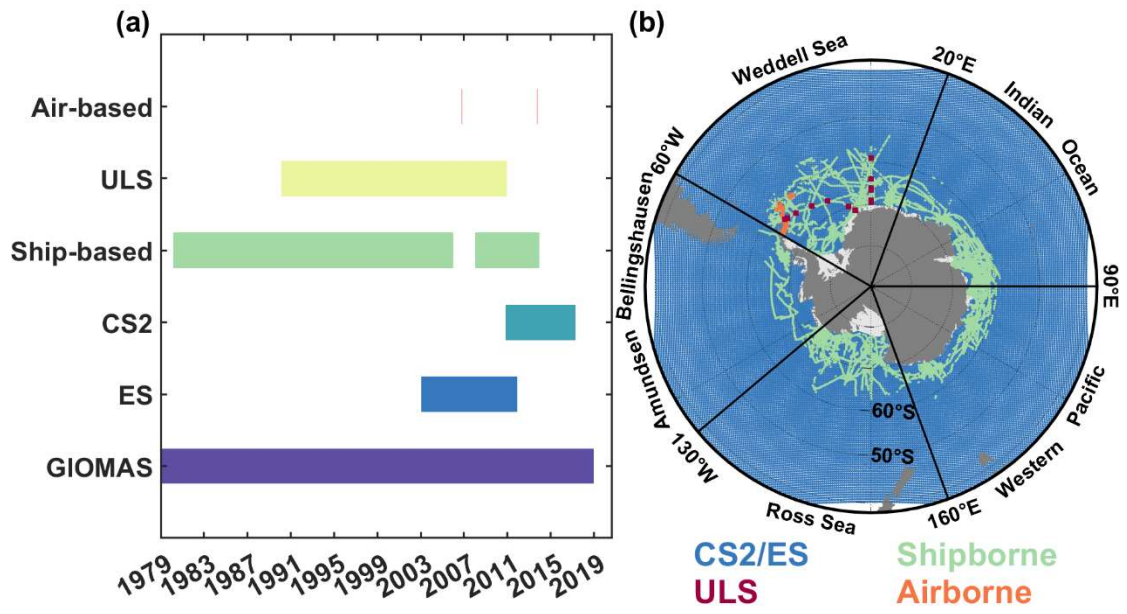
594 Yang, Q., Losa, S. N., Losch, M., Tian-Kunze, X., Nerger, L., Liu, J., Kaleschke, L., and Zhang, Z.:
595 Assimilating SMOS sea ice thickness into a coupled ice-ocean model using a local SEIK filter, *J.*
596 *Geophys. Res.-Oceans*, 119, 6680-6692, <https://doi.org/10.1002/2014jc009963>, 2014.

597 Yang, Q., Losa, S. N., Losch, M., Liu, J., Zhang, Z., Nerger, L., and Yang, H.: Assimilating summer sea-
598 ice concentration into a coupled ice-ocean model using a LSEIK filter, *Ann. Glaciol.*, 56, 38-44,
599 <https://doi.org/10.3189/2015AoG69A740>, 2015.

600 Zhang, J., and Rothrock, D. A.: Modeling global sea ice with a thickness and enthalpy distribution model
601 in generalized curvilinear coordinates, *Mon. Weather Rev.*, 131, 845-861, [https://doi.org/10.1175/1520-0493\(2003\)131<0845:Mgsiwa>2.0.Co;2](https://doi.org/10.1175/1520-0493(2003)131<0845:Mgsiwa>2.0.Co;2), 2003.

602
603 Zhang, J.: Increasing Antarctic Sea Ice under Warming Atmospheric and Oceanic Conditions, *J. Climate*,
604 20, 2515-2529, <https://doi.org/10.1175/jcli4136.1>, 2007.

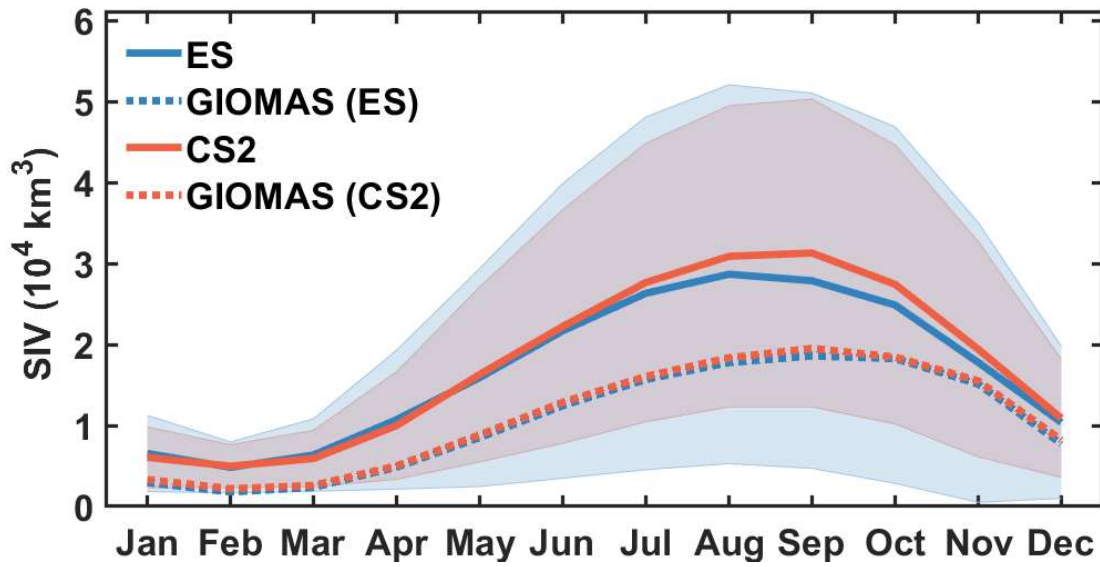
605



606

607 **Figure 1.** (a) The temporal and (b) spatial coverage of data used in this study.

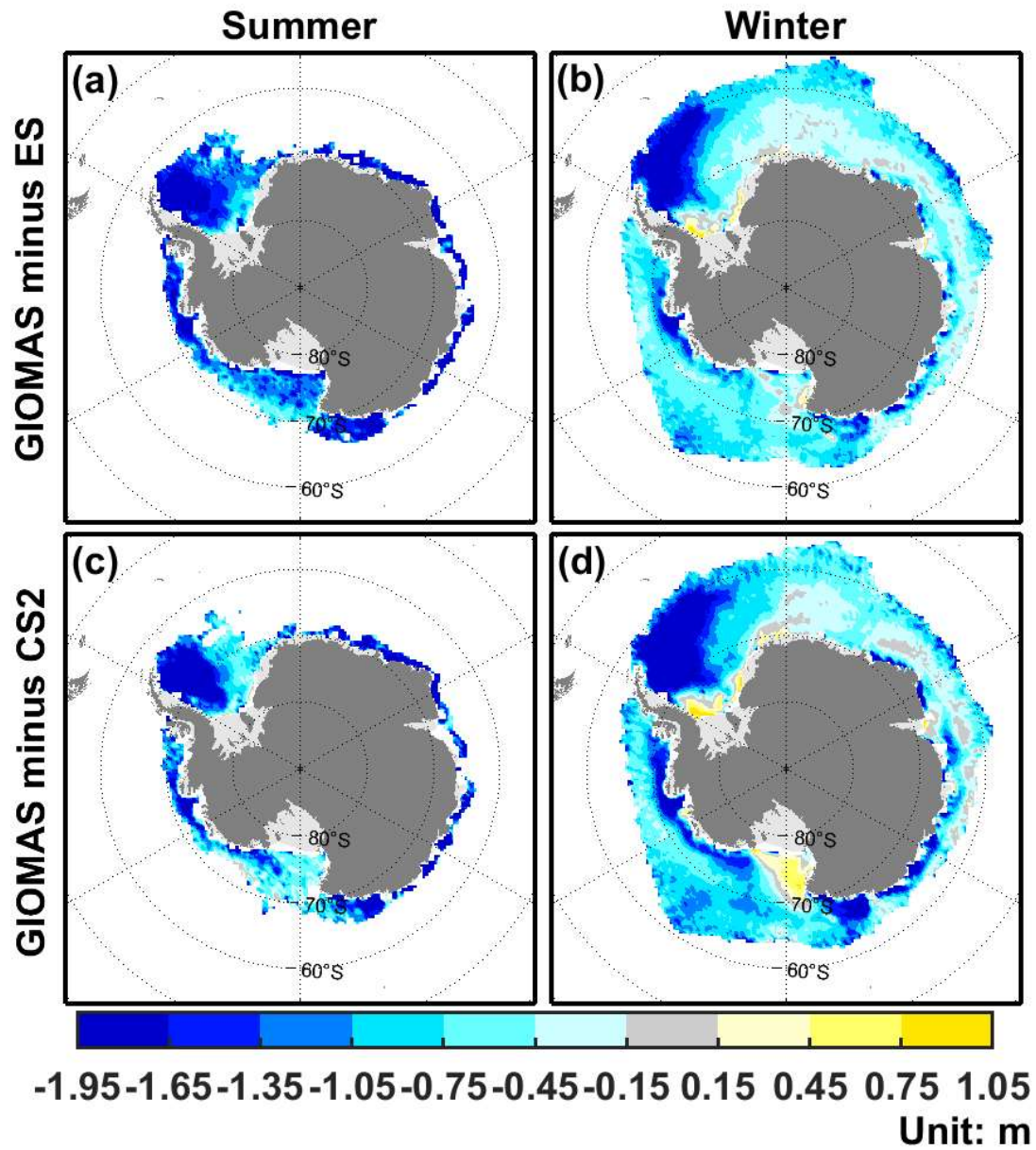
608



609

610 **Figure 2.** The climatological annual cycle of Antarctic SIV. The blue and red denote data related to ES
 611 and CS2, respectively. The solid and dashed curves denote satellite observations and corresponding
 612 GIOMAS data.

613

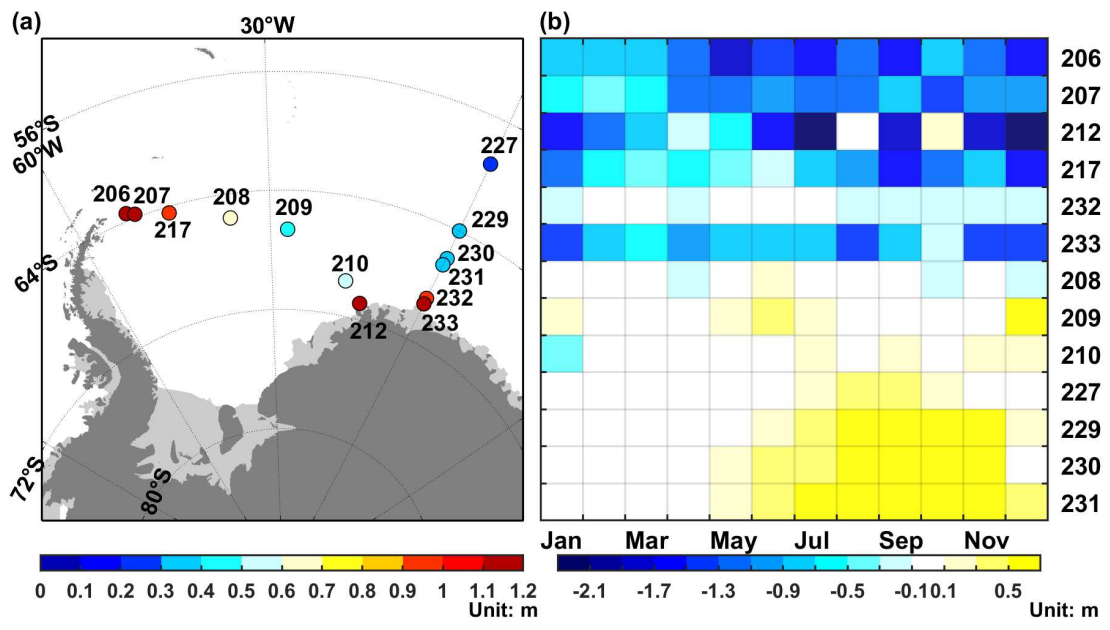


614

615 **Figure 3.** The SIT bias of GIOMAS relative to ES in (a) the summer and (b) winter. (c-d) same as (a-b)

616 but for bias relative to CS2.

617

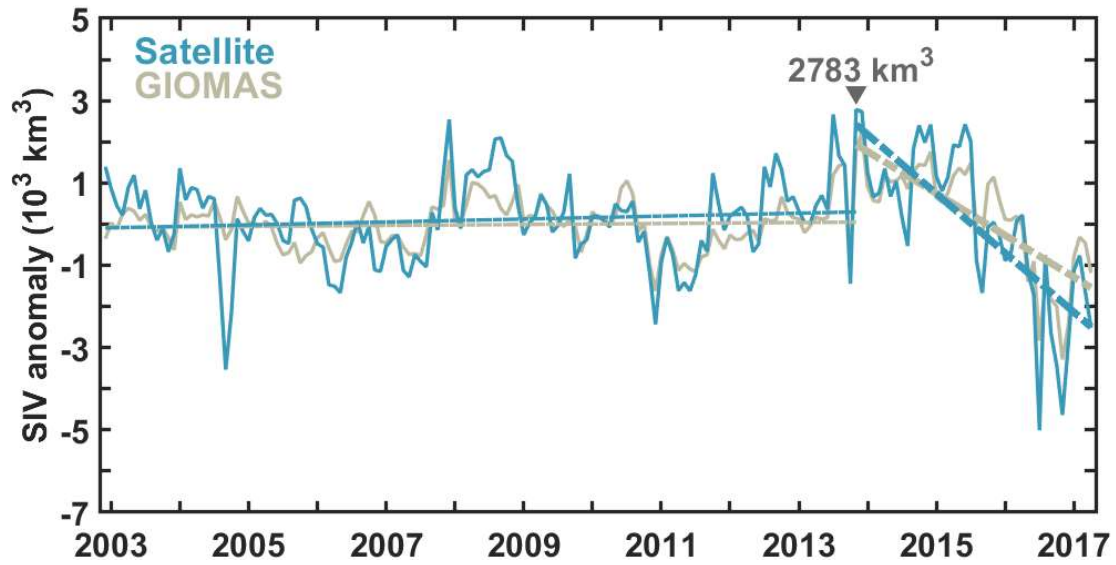


618

619 **Figure 4.** (a) The locations of ULS in the Weddell Sea and corresponding standard deviation of SIT. (b)

620 The differences in SIT climatology between GIOMAS and ULS.

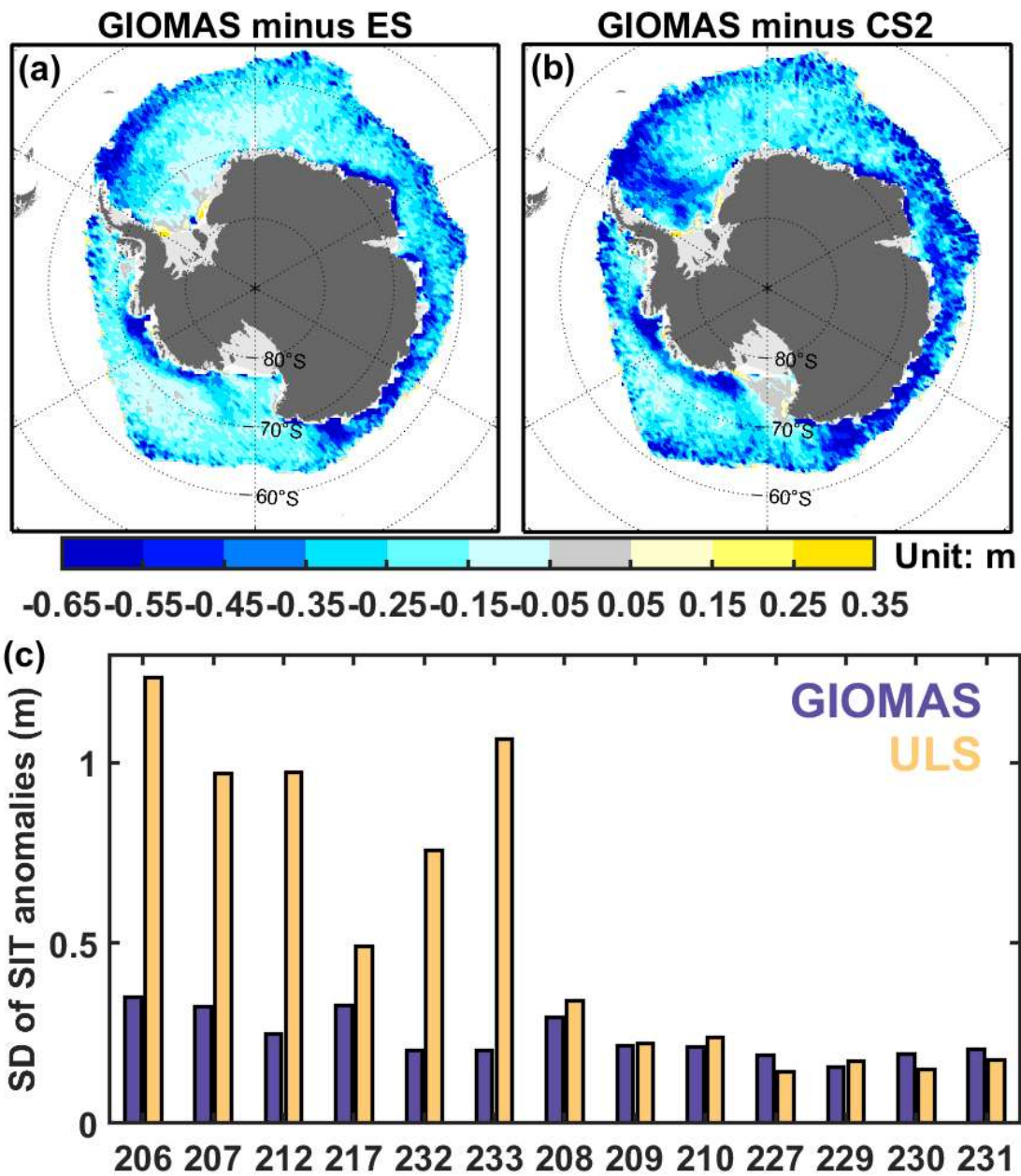
621



622

623 **Figure 5.** The SIV anomalies of satellite observations (green) and corresponding GIOMAS (khaki). The
 624 dashed lines denote the linear trends of SIV anomalies from December 2002 to November 2013 and from
 625 November 2013 to April 2017. All linear trends have passed a F-test at 99% significant level.

626



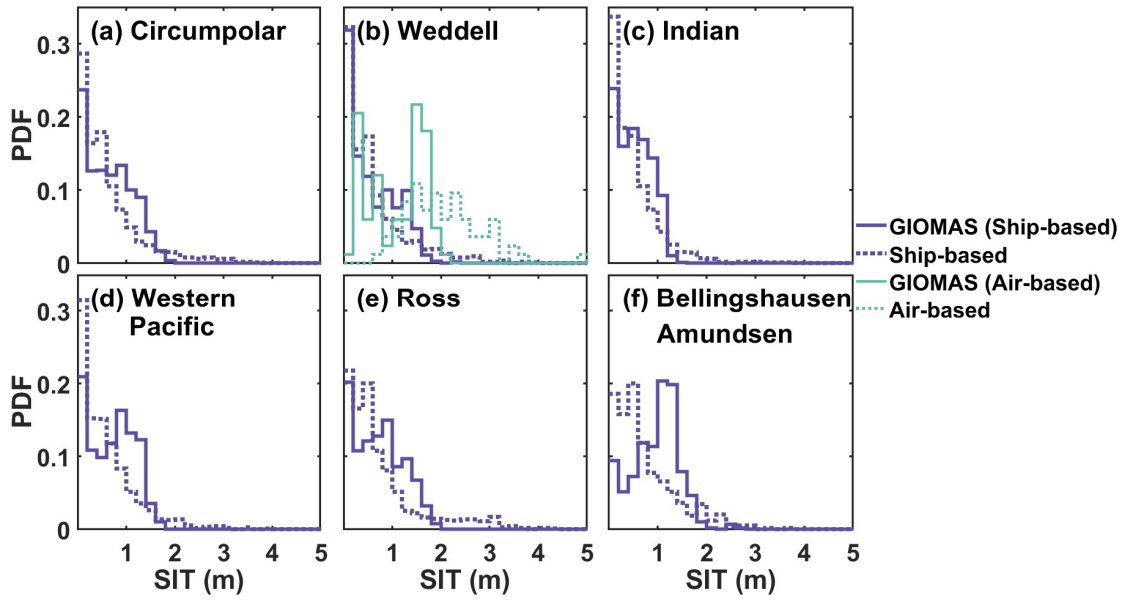
627

628 **Figure 6.** (a) The spatial differences in standard deviation of SIT anomalies between GIOMAS and ES.

629 (b) same as (a) but for differences between GIOMAS and CS2. (c) The standard deviation of SIT

630 anomalies for ULS (yellow) and corresponding GIOMAS (blue).

631



632

633 **Figure 7.** SIT histograms of GIOMAS and in situ observations in (a) the Southern Ocean and (b-f)

634 different sectors.